Energy & Environmental Science

Cite this: *Energy Environ. Sci.*, 2011, **4**, 2177

www.rsc.org/ees

PAPER

Carbon capture in metal–organic frameworks—a comparative study†

Jason M. Simmons,*[a] Hui Wu,[ab] Wei Zhou[ab] and Taner Yildirim[ac]

Received 22nd November 2010, Accepted 15th March 2011
DOI: 10.1039/c0ee00700e

Metal–organic frameworks (MOFs) have been shown to be excellent materials for storage of carbon dioxide, implying that they could be useful for removal of carbon dioxide from flue gas stacks, however their performance in industrially relevant swing adsorption processes for carbon capture has not been studied. Here we show that the efficacy of MOFs for carbon capture depends dramatically on the process and that some MOFs can provide significant carbon capture under typical pressure and vacuum swing processes. In particular, MOFs that possess coordinatively unsaturated metal centers offer as much as 9 mmol g^{-1} swing capacity under certain conditions. The results herein clearly show that there is no single ideal compound for carbon capture applications and that different materials can perform better or worse depending on the specific process conditions. In addition to their capture performances, we have also investigated their selectivity to carbon dioxide over that of nitrogen and methane. The analysis provided clearly demonstrates that the performance of a given MOF cannot be determined without also considering the detailed industrial process in which the MOF is to be applied.

Introduction

Concerns over the role of anthropogenic carbon dioxide in global climatic change have led to increasing interest in carbon mitigation schemes.[1,2] In particular, the increasing concentration of carbon dioxide in the atmosphere is believed to be a primary factor in the increased global mean temperature. Much of the anthropogenic carbon dioxide emissions are the direct result of the use of hydrocarbons both as fuels and in industrial processing but, given their abundance and relatively low cost, hydrocarbons will continue to be used in the foreseeable future. Therefore, the minimization of carbon emissions will require effective carbon capture and sequestration technologies.

Metal–organic frameworks (MOFs) and coordination polymers have recently been investigated for a wide range of applications, most extensively for their ability to store energy-related gases including hydrogen and methane.[3,4] In addition to reducing CO_2 emissions through alternative fuels, MOFs can directly adsorb significant amounts of CO_2.[5] In certain situations, ultra-high surface area MOFs have been shown to store nearly ten times more CO_2 at high pressure than an empty cylinder alone.[5,6] In addition, incorporation of preferred binding sites, such as

[a]*NIST Center for Neutron Research, National Institute of Standards and Technology, Gaithersburg, Maryland, 20899-6102, USA. E-mail: jason.simmons@nist.gov*
[b]*Department of Materials Science and Engineering, University of Maryland, College Park, Maryland, 20742-2115, USA*
[c]*Department of Materials Science and Engineering, University of Pennsylvania, Philadelphia, Pennsylvania, 19104-6272, USA*

† Electronic supplementary information (ESI) available: Diffraction pattern for ZIF-8, temperature dependent CO_2 isotherms for all MOFs, details of IAST calculations, a comparison of room temperature CO_2, CH_4 and N_2 isotherms for each MOF, and an alternative plot of isosteric heat of adsorption. See DOI: 10.1039/c0ee00700e

Broader context

Carbon capture is a critical component of the mitigation of CO_2 emissions from industrial plants. Investigations of the application of metal–organic frameworks (MOFs) to adsorptive carbon capture have focused on their appreciable storage capacities but fail to address the more pertinent issue of how MOFs perform under common industrial separation processes that are at the heart of carbon capture. Typical processes rely on swing adsorption and are limited to relatively low CO_2 partial pressures such that the total pore volume and the surface area are under-utilized. Here, we investigate the performance of a number of metal–organic frameworks with particular focus on their behavior at the low pressures commonly used in swing adsorption. The MOFs chosen include those with high surface areas and different pore geometries, as well as some MOFs that contain enhanced binding sites. This comparison clearly shows that it is the process that determines which MOF is optimal rather than there being one best MOF, though MOFs that possess enhanced binding at open metal sites generally perform better than those with high surface area. At the low pressures used in swing adsorption processes, the binding energy is most important and not the total pore area or volume.

coordinatively unsaturated metal sites or amine functionalities, can greatly increase the isosteric heats of adsorption.[7–10] While these results are impressive, they do not address the longer term issues of storage, for which terrestrial carbon sequestration is believed to be more viable.[2]

Though MOFs may not be practical for sequestration, they hold great promise for the initial capture of CO_2 from post-combustion flue gas emissions. The current technology relies on highly caustic amine-based solvents to absorb CO_2, followed by high temperature regeneration. While effective, liquid amines suffer from degradation during regeneration and present a significant parasitic load on a power plant, on the order of 25% to 40% of the energy generated.[2] An alternative method utilizes highly porous materials to selectively adsorb the CO_2 and allow the non-hazardous gases to escape. To effectively remove the CO_2, the systems will typically use pressure or vacuum swing adsorption (PSA/VSA) techniques, adsorbing CO_2 at modestly elevated pressures and releasing it to a storage tank at lower pressures. PSA systems typically adsorb at inlet pressures near 6 bar and desorb at 1 bar whereas VSA uses an inlet pressure of ~1.5 bar and will evacuate to ~0.05 bar for desorption.[11] Swing sorption processes are often implemented in multiple stages in order to increase the overall capture/separation efficiencies.[12] PSA/VSA techniques are commonly used for natural gas upgrading (removal of CO_2 from CH_4) as well as for CO_2 capture and rely on large uptakes over a narrow pressure range. Due to the modest pressures used in PSA/VSA techniques, knowledge about the high pressure capacity of a given framework is of little use; it is the performance under low inlet pressures that is important. This is particularly the case in separation processes where the partial pressure of the target gas, for example 10% to 20% CO_2 in flue gas, that must be taken into account Thus, in a PSA/VSA process, a delicate balance must be had between strength of CO_2 adsorption, working capacity and selectivity towards CO_2 over other potential impurities.

While there have been numerous comparative studies of MOFs for high pressure CO_2 storage,[5,6,12] comparisons of their properties in technologically relevant capture processes have been somewhat lacking.[14–16] Here we discuss the CO_2 sorption behaviours of several MOF materials with an eye towards their potential application in PSA/VSA carbon capture processes. We have chosen a wide range of MOF materials to provide the widest body of comparison, including common high surface area MOFs and several that contain open, coordinatively unsaturated metal sites that have been shown to offer an increased binding energy to other gases such as H_2 and CH_4,[17,18] in addition to CO_2.[9] Detailed sorption measurements are used to determine CO_2 storage capacity as a function of temperature and to extract the energetics of adsorption. In addition, these measurements enable the determination of the usable sorption capacity under PSA/VSA conditions, which are compared to other MOFs in the literature. Finally, we address the role of flue gas impurities by calculating the CO_2/CH_4 and CO_2/N_2 selectivity from experimentally measured sorption isotherms. It is important to note, however, that the purpose of this work is not only to comment on the potential utility of these MOFs, but rather to address the wider issues about how to best compare the performance of MOFs by also including the detailed processes in which a MOF is to be applied.

Experimental

We have chosen two prototypical MOFs, namely MOF-5 [Zn_4O(benzenedicarboxylate)$_3$],[19] and ZIF-8 [Zn(methylimidazolate)$_2$],[20] as representative of samples whose properties are largely determined by their surface area and pore geometries. For the coordinatively unsaturated metal site MOFs, we have focused on three MOFs with copper paddle-wheel nodes possessing an open Cu(II) site, PCN-11 [Cu_2(*trans*-stilbenetetracarboxylate)],[21] PCN-16 [Cu_2(ethynediyl-bis(benzenedicarboxylate))],[22] and HKUST-1 [Cu_3(1,3,5-benzenetricarboxylate)$_2$],[23,24] as well as the magnesium and zinc variants of MOF-74 [M_2(2,5-dioxidoterephthalate), M = Mg, Zn, also known as CPO-27-M],[25–27] which has an open M(II) site.

All MOF samples were synthesized based on methods reported in the literature and, with the exception of ZIF-8, were the exact same samples as those used in earlier studies of H_2 and CH_4 storage.[21,22,24,28–30] These samples were thoroughly characterised using both nitrogen physisorption and diffraction techniques in the cited references. In the case of ZIF-8, the sample contained a 1 : 1 Zn to Co ratio and was determined to be isostructural and possesses indistinguishable gas sorption properties compared to that of a pure Zn-ZIF-8 (see Fig. S25†).[18] All samples have been thoroughly outgassed to remove residual solvents and sample handling is performed in a He glove box. Gas sorption measurements were performed on a computer controlled Sieverts apparatus, details of which have been published elsewhere.[31] All gases are of Research or Scientific grade, with a minimum purity of 99.999%. Isosteric heats of adsorption are calculated from the Clausius–Clapeyron equation using isotherms in the range of 220 K to 310 K.[31] Gas selectivity calculations are performed using experimentally measured isotherms within the Ideal Adsorbed Solution Theory (IAST) of Myers and Prausnitz,[32] a method that has been shown to be valid for other MOF materials.[33–36]

Results and discussion

Crystal structures and salient pore metrics for the MOFs under consideration are shown in Fig. 1 and Table 1, respectively. MOF-5, as is well known, possesses a largely open pore within a simple cubic framework of Zn_4O nodes and benzene-dicarboxylate struts. This open structure allows for relatively high surface area and facile diffusion of molecules into the pore. In ZIF-8, M-N_4 (M = Zn, Co) tetrahedra are joined through imidazolate rings resulting in a similar pore size to that of MOF-5 (~11 Å), however there are more pore entrances, each of which is smaller than that of MOF-5. PCN-11, PCN-16 and HKUST-1 possess a common copper paddle-wheel node, coupled through extended multi-carboxylate ligands. The PCN structures contain two types of pores; one relatively small spherical cage of ~7 Å, and the other an elliptical cage extended along the *c*-axis. In the case of HKUST-1, there are three nearly spherical pores with 4, 10, and 11 Å dimensions. M–MOF-74 is different than the other MOFs measured here in that it does not possess enclosed pores; rather it consists of a hexagonal array of long cylindrical channels, with the metal nodes forming stripes down the length of the channel. At the low pressures under consideration for PSA/VSA processes, where the density of the adsorbed gas is expected to be

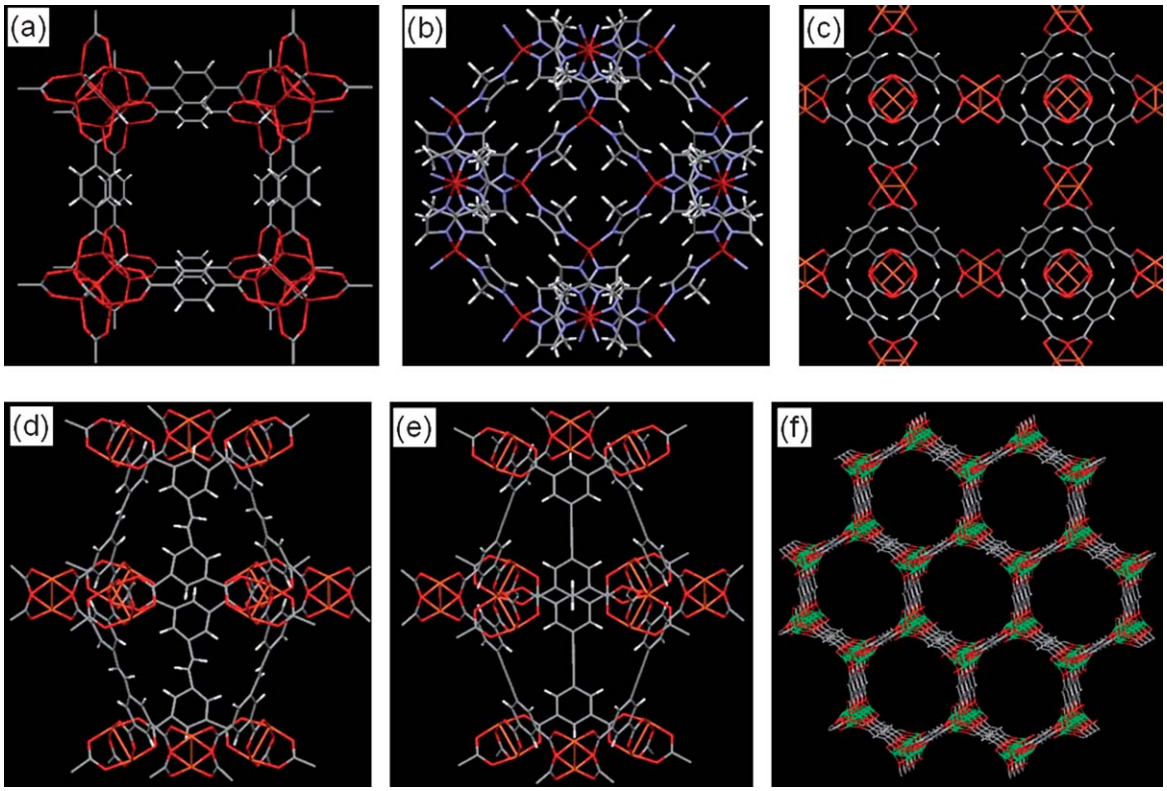

Fig. 1 Crystal structures for MOFs under investigation: (a) MOF-5, (b) ZIF-8, (c) HKUST-1, the elliptical pore of (d) PCN-11 and (e) PCN-16, and (f) 1-D hexagonal channels of MOF-74. Color code: carbon (grey), hydrogen (white), oxygen (red), nitrogen (blue), zinc/cobalt (maroon), copper (orange) and magnesium (green).

relatively low, the presence of enclosed pores is unlikely to offer significant advantage as compared to the channels in MOF-74. Post-synthesis dehydration of the PCNs, HKUST-1 and M–MOF-74 yields the unsaturated metal site.

Temperature dependent CO_2 sorption isotherms for two representative MOFs, MOF-5 and PCN-11, are shown in Fig. 2. Corresponding isotherms for the other MOFs are included in the ESI† (Fig. S1–S7). Included in Fig. 2a is the room temperature CO_2 sorption isotherm measured by Millward and Yaghi,[5] showing excellent agreement with our measurements. Also included in Fig. 2c is a comparison of the CO_2 sorption isotherms for all measured materials at room temperature. All isotherms show complete reversibility, consistent with a largely physisorptive process. Certain MOFs, in particular MOF-5 and PCN-11, have been measured multiple times without any indication of loss of capacity. Estimated errors including both sample repeatability and instrumental resolution are no more than 5%. The full reversibility and repeatability of the measured isotherms imply that the MOFs should show little degradation of performance in swing adsorption cycling.

MOF-5 shows a rather unique S-shaped sorption isotherm, the cause of which is not fully understood but may arise from the confinement of CO_2 in the MOF pores leading to a locally increased CO_2 density.[37,38] Close inspection of the ZIF-8 isotherm shows a similar though less pronounced S-shape, suggesting a similar adsorption mechanism. In contrast, PCN-11 has

Table 1 Structural parameters of the investigated MOFs[a]

Structure	BET surface area/m^2 g^{-1}	Pore volume/cm^3 g^{-1}	Pore dimensions/Å	Reference
PCN-11	1931	0.91	7; 11 × 16	21
PCN-16	2273	1.06	7; 11 × 16	22
HKUST-1	1690	0.66	4; 10; 11	—
Mg–MOF-74	1332	0.61	11 × 11 channel	28
Zn–MOF-74	885	0.41	11 × 11 channel	28
ZIF-8	1980	0.65	11.6	—
MOF-5	3500	1.31	12	—

[a] References are for previous works using the exact same samples in which the nitrogen sorption analysis was performed. Other values determined from 77 K N_2 isotherms, with BET area calculated between $P/P_o = 0.005$ and 0.03 and pore volume is calculated at $P/P_o = 0.75$. All values are consistent with reported values in the literature.

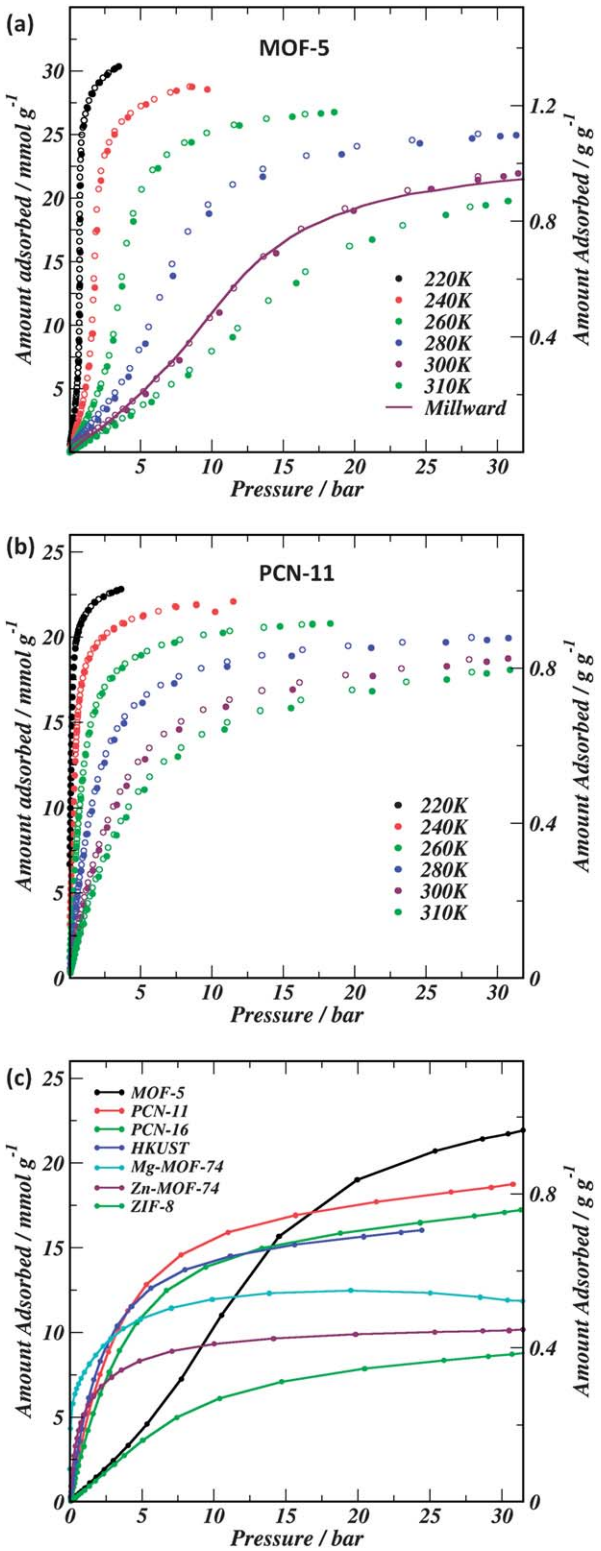

Fig. 2 Temperature dependent excess CO_2 sorption isotherms for (a) MOF-5 and (b) PCN-11. The solid (open) symbols represent the adsorption (desorption) branch. The solid line in (a) is the room temperature isotherm reported by Millward and Yaghi.[5] (c) Room temperature (300 K) isotherms for all MOFs investigated. Estimated errors are <5%. MOFs with open metal centers show larger initial uptake but have relatively lower saturation uptakes due to their lower available surface area.

a typical type-I like sorption curve, with significant sorption at low pressures. At high pressures, the saturation uptake measured for each material correlates reasonably well with the apparent surface area and pore volume, though the presence of the open metal site can lead to higher adsorbed gas densities and therefore higher capacity as compared to samples without such sites.[39]

Although MOF-5 has an impressive room temperature uptake at elevated pressures and can store more than any of the other MOFs measured here, the specific curvature in the isotherm makes it much less applicable to low pressure sorption in general and to PSA/VSA processes in particular; it is only at pressures above 10 bar that there is a significant derivative in the isotherm and above 15 bar that its uptake exceeds that of PCN-11. This difference is clear from the calculated isosteric heats of adsorption for each material, shown in Fig. 3. Though MOF-5 has a higher saturation capacity, CO_2 is much less strongly bound across the entire sorption curve. At low loadings, the MOFs that possess open metal centers (PCN-11, PCN-16, HKUST-1, M–MOF-74) show significantly higher isosteric heats as compared to the fully coordinated metal MOFs (MOF-5, ZIF-8). Recent diffraction results and DFT calculations clearly show that the open metal sites are the primary CO_2 adsorption sites and lead to this enhanced isosteric heat.[40,41] At high loadings, the extracted isosteric heats begin to increase but show a similar slope. To make sense of the shape of the isosteric heat curves, it is important to remember that the isosteric heat is a combination of sorbate–sorbent (gas–surface) and sorbate–sorbate (gas–gas) interactions. The gas–surface interactions generally decay with loading as the stronger bound sites are filled, leaving less favorable binding sites for subsequent gas molecules. This is most clear in Zn–MOF-74 where there is a low-uptake plateau up to ~5 mmol g^{-1} where the CO_2 is interacting with the open metal center (6 mmol g^{-1} ≈ 1 CO_2 per Zn(II)), then decreases as the secondary sites are filled. In contrast, the gas–gas interactions

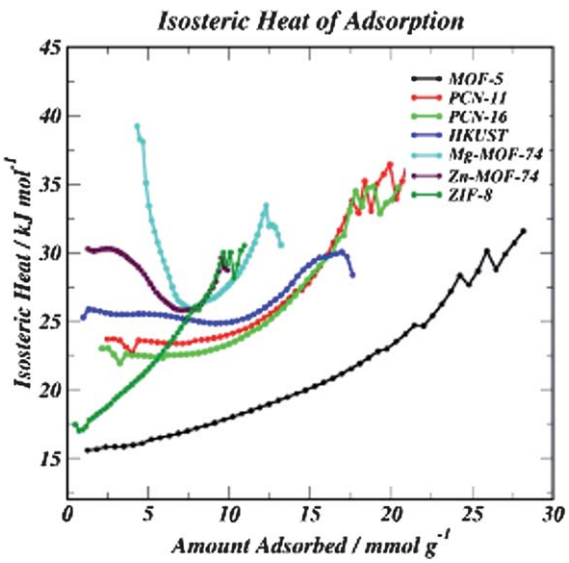

Fig. 3 Calculated isosteric heat of CO_2 adsorption as a function of uptake. Materials with open metal centers show consistently higher isosteric heats of adsorption for each uptake. The upward sweep at high loadings indicates the dominance of the CO_2–CO_2 interactions over the CO_2–MOF binding.

tend to increase with pressure as the density of the gas increases, pushing the molecules closer together.[42] For the open-metal center MOFs, the CO_2–M(II) site interaction is dominant at low pressures/uptakes, and it is only at higher pressures where the CO_2–CO_2 interactions are apparent. The curves for MOF-5 and ZIF-8 are distinctly different in that they tend to increase uniformly with pressure, indicating that the CO_2–MOF interaction is quite weak such that the CO_2–CO_2 gas phase interactions are important even at relatively low uptakes.

As mentioned above, high saturation capacities and large isosteric heats of adsorption are only inherently useful for storage applications. While MOFs may be useful for some storage applications, their role in carbon dioxide mitigation is more likely directed towards the initial capture of CO_2 rather than for long term sequestration. For most processes, there is a trade-off between the performance of the material and the ultimate cost for that performance. In most industrial applications, such as flue gas scrubbing and natural gas upgrading, there is a limited range of process parameters that are considered commercially viable and are typically limited to the low pressure and modest temperature regimes. Considering the PSA and VSA processes, it is more important to focus on the amount of CO_2 that can be effectively removed from the system under low pressure swing operations. Using the room temperature isotherms shown in Fig. 2c, we can estimate the PSA/VSA capacities under ideal conditions, as illustrated in Fig. 4a. The capture capacity is defined as the difference in adsorbed amount between the high and low pressure extremes of the swing process. This is the amount of gas that is adsorbed during the initial pressurization stage of the cycle, less the amount that remains in the MOF under the low pressure present in the desorption stage that is sent for ultimate sequestration. For the PSA process indicated in Fig. 4a, the capture capacity is estimated by the difference in the amount adsorbed between 6 bar and 1 bar: $N(P = 6\ \text{bar}) - N(P = 1\ \text{bar})$. Of course, in a real flue gas, CO_2 is only a fraction of the stream, typically on the order of 10% to 20%, with N_2 as the primary component. For the flue gas case, we have chosen a 20% CO_2 gas stream such that we estimate the capacity based on the CO_2 partial pressures which are 1.2 bar to 0.2 bar (PSA) and 0.3 bar to 0.01 bar (VSA). Both pure CO_2 and flue gas cases are presented because these values represent the range of CO_2 capture that could be achieved in a multi-step separation process where the CO_2-enriched stream from a first separation stage is fed into subsequent stages.

Fig. 4b and c show the low pressure region of the room temperature isotherms that is relevant for the PSA (VSA) process. The specific capacities extracted from these graphs are presented in Table 2, along with similarly estimated capacities based on literature reports of MOFs and other high surface area materials. In addition to presenting data for the capture efficiencies based on a pure CO_2 gas stream, Table 2 also shows the estimated capacities assuming a 20% partial pressure of CO_2 in a hypothetical flue gas stream. Though competitive adsorption of other gases will reduce the CO_2 capture capacity from the flue gas, the room temperature uptake of N_2, the primary component of the flue gas, is relatively small in most MOFs and is ignored in these swing adsorption estimates. However, it should be noted that the estimated capture capacity could be reduced further by other impurities in the flue gas, in particular water, which are present at much lower concentrations.

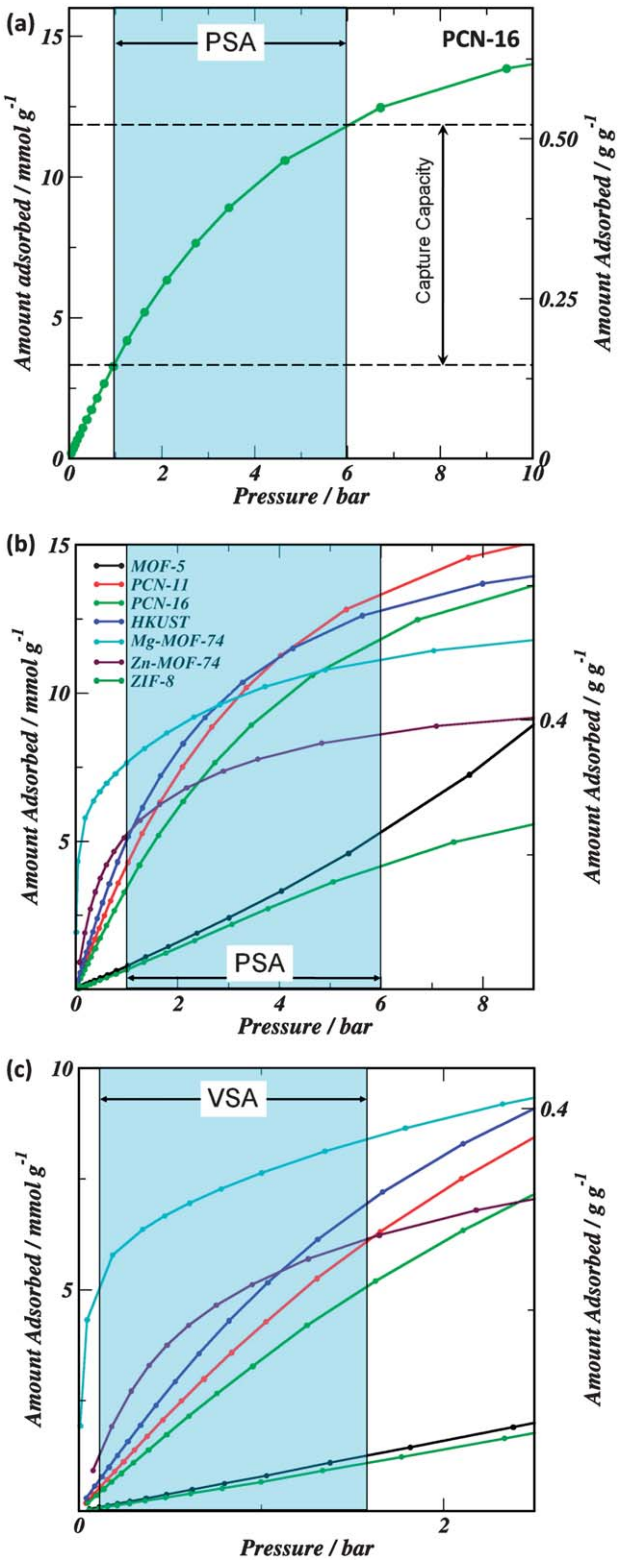

Fig. 4 (a) Schematic of the determination of swing adsorption capture capacity as illustrated for a PSA process using PCN-16. The capacity is defined to be the difference in uptake between the high (6 bar) and low (1 bar) pressure extremes for each process. For VSA, the pressure ranges from 1.5 bar to 0.05 bar. (b) PSA and (c) VSA region of the isotherms shown in Fig. 2c highlighting the differences between the MOFs in each process.

Table 2 Swing adsorption capacities:[a] estimated room temperature swing adsorption capacities in mmol g^{-1} for a range of porous materials, including the MOFs studied in this work as well as MOFs and zeolites determined from isotherms reported by others. Estimated error for the samples measured in this work is <5% for uptakes and ±0.5 kJ mol^{-1} for isosteric heat. Values are estimated for both a pure CO_2 gas stream (1 bar to 6 bar PSA; 0.05 bar to 1.5 bar VSA) and a 20% partial CO_2 pressure flue gas (0.2 bar to 1.2 bar PSA; 0.01 bar to 0.3 bar VSA). The MOFs with the highest capacities for each column are listed in italics

	Pure CO_2		Flue gas			
Structure	PSA/mmol g^{-1}	VSA/mmol g^{-1}	PSA/mmol g^{-1}	VSA/mmol g^{-1}	Q_{st}/kJ mol^{-1}	Reference
PCN-11	*9.1*	*5.6*	*4.0*	1.4	23	This work
PCN-16	*8.5*	4.6	3.3	1.1	22.5	This work
HKUST-1	7.8	*6.4*	*4.5*	1.6	26	This work
Mg–MOF-74	3.5	3.9	2.1	*4.1*	45	This work
Zn–MOF-74	3.5	*5.4*	*3.6*	2.7	30	This work
MOF-5	4.4	1.2	0.7	0.2	15	This work
ZIF-8	3.4	1.0	0.7	0.2	17	This work
HKUST-1	4.4	4.0	3.5	—	28.1	15
	6.5	—	3	—	—	43
CPO-27 series (Mg,Ni,Zn,Co)	—	3.6	2.0	*4.7*	50–20 (Mg)	9*
	—	*5.6*	3.1	*4.5*	35(Co)	
	—	4.3	2.5	3.4	40–30 (Ni)	
	—	4.9	3.2	2.9	— (Zn)	
Ni-STA-12	2.6	3.7	3.0	0.8	30	44
MIL-100	4.2	—	—	—	60	6
MIL-101	*9.0*	—	—	—	45	6
MOF-508	5.0	2.0	1.6	0.7	15–20	45
Zeolite 13X	1.6	2.8	1.8	2.5	37	46
	1.3	—	—	—	—	43
NaX	—	4.4	1.3	2.4	50	47
CuBTTri-en	—	0.9	0.7	0.5	80–30	8*
CuBTTri	—	3.7	3.0	1.3	20	8*
Zn-Atz-oxalate	—	1.7	1.1	2.2	40	10*
ZIF-78	—	1.8	1.3	1.2	—	13*
ZIF-95	—	0.9	0.7	0.3	—	48*
ZIF-100	—	0.9	0.7	0.4	—	48*
H-ZSM-5	—	1.2	0.9	—	—	49*

[a] Values that could not be determined from the published reports are designated as (—). References marked by a asterisk (*) only report data up to 1 bar pressure, which was used for the upper limit on the respective swing uptakes. Isosteric heats of adsorption are included if reported in the original paper.

Of the MOFs studied here, PCN-11 shows the highest theoretical capacity under pure-CO_2 PSA conditions while HKUST-1 is slightly more useful in a VSA process. Also important to note is that a material that shows only limited applicability under one set of conditions may be more useful under different conditions. For example, Zn–MOF-74 has the lowest PSA capacity of the MOFs studied here but is one of the best under VSA conditions. As is readily seen, the capture capacity for MOF-5 is considerably lower than other materials, particularly under VSA conditions even though it possesses the highest surface area and largest saturation storage capacity. Comparing across literature reports in Table 2, PCN-11 still shows the best PSA capacity, but is only slightly higher than MIL-101 and PCN-16. For pure CO_2 VSA conditions, HKUST-1 exceeds the uptake of any other material by nearly 1 mmol g^{-1}, followed by PCN-11 and two of the MOF-74 variants.

In the case of the 20% CO_2 flue gas, the roles change somewhat. HKUST-1 offers the highest PSA uptake, 4.5 mmol g^{-1}, across the 0.2 bar to 1.2 bar partial pressure of CO_2 in the gas. However, the PSA swing capacity of HKUST-1 only slightly larger than PCN-11 at 4.0 mmol g^{-1} and Zn–MOF-74 at 3.6 mmol g^{-1}. Again, HKUST-1 and PCN-11 far exceed the other MOFs listed in Table 2. Under flue gas VSA conditions, the large isosteric heat of adsorption seems to favor Mg–MOF-74, as well as the Co–MOF-74 variant measured by Caskey *et al.*[9] Indeed, the MOF-74 variants exceed the next best materials by as much as 2 mmol g^{-1}, nearly double the ~2.5 mmol g^{-1} capacity of zeolites 13X and NaX. In addition to reiterating the importance of matching the material to the process conditions, these results show that it may be possible to improve the overall efficiency of a multi-stage separation process by using different sorptive materials in each stage, for example using Mg–MOF-74 for an initial low partial pressure VSA stage and PCN-11 under PSA conditions for the CO_2-enriched later stages.

Taken as a whole, these results clearly show the importance of matching a material to the process. Indeed, this concept is well known to the hydrogen storage community as illustrated by the competing H_2 storage targets developed by the DOE. In the case of hydrogen, these concepts have been well explained by Bhatia and Myers[50] and others[51] in order to determine the optimal material for a given set of pressure/temperature conditions. Bhatia and Myers clearly showed that an optimal hydrogen storage material would have an isosteric heat of adsorption near 20 kJ mol^{-1} given the 1 bar to 35 bar range of pressure that was considered. Using the same methodology, we can make a similar estimate for CO_2 under PSA and VSA conditions. Assuming a Langmuir-type isotherm model, the optimal isosteric heat of adsorption can be estimated to be (eqn 4 from Bhatia and Myers)

$$-Q_{st} = \Delta H^{o}_{opt} \approx T\Delta S^{o} + \frac{RT}{2}\ln\left(\frac{P_1 P_2}{P_0}\right),$$

where R is the gas constant, T is temperature, P_1 and P_2 are the high and low (partial) pressure limits of the process, and ΔS^{o} is the entropy change upon adsorption. Typical values of the change of entropy change upon CO_2 adsorption on other porous materials are between -65 J mol^{-1} K^{-1} and -100 J mol^{-1} K^{-1}.[49,52,53] Taking $\Delta S^{o} \approx -80$ J mol^{-1} K^{-1}, for PSA processes between 6 bar and 1 bar pressures at room temperature, $\Delta H^{o} \approx -22$ kJ mol^{-1}. Similarly, $\Delta H^{o} \approx -28$ kJ mol^{-1} for a VSA process. For the modified PSA/VSA conditions, assuming a 20% CO_2 flue gas, the values are $\Delta H^{o} \approx -26$ kJ mol^{-1}– and $\Delta H^{o} \approx -31$ kJ mol^{-1}, respectively. Comparing these numbers to those shown in Fig. 3 and in Table 2, we clearly see that materials with isosteric heats closest to these estimated optimal values do indeed show the best swing adsorption capacity. Ultimately, it is the balance of enthalpy and available surface area that will lead to the best performing material.

Finally, industrial application of MOFs to carbon capture will require not only optimization of the MOF for a given set of temperature and pressure conditions but also discrimination of, and tolerance to, the common impurities in typical flue gases which contain not only CO_2, but also N_2, CH_4, and water along with numerous other gases. In particular, the selectivity of the MOF is critical to maximize the capacity of CO_2 stored so that precious sorption sites are not taken up by non-CO_2 molecules. As an initial step, we have investigated the selective adsorption of CO_2 over CH_4 and N_2 in several MOFs. Both separations are important for CO_2 capture from flue gas while CO_2 separation from CH_4 is also important in natural gas refining. The selectivity is calculated using IAST theory[32] which explicitly takes into account the competitive adsorption of different gases. Details of the IAST computation and the experimental isotherms used to calculate the selectivity are presented in the ESI† (Section SIIa and Fig. S11–S22). The results of the IAST selectivity calculations near room temperature (300 K to 310 K) are shown in Fig. 5; results for lower temperatures (280 K to 290 K) are given in the ESI† (Fig. S8–S10). What is immediately clear is that, similar to the results for the swing sorption capacities, MOFs that possess open metal sites demonstrate the largest selectivities. For CO_2/CH_4 selectivity (Fig. 5a and b), Mg–MOF-74 shows a selectivity of ~175 at low pressure, similar to recently reported values based on the ratio of Henry constants,[54,55] while the other open metal center MOFs show selectivities between 5 and 13. The value for HKUST-1 is in quantitative agreement with another recent work.[56] Both MOF-5 and ZIF-8, materials that depend on their high surface areas for their storage capacities, show much more modest selectivities on the order of 2.5. In the case of CO_2/N_2 selectivity (Fig. 5c), the contrast is even larger. The room temperature nitrogen sorption in Mg–MOF-74 is too low to apply IAST to for the pressure ranges we have used while Zn–MOF-74 shows a selectivity of 35. Again, MOF-5 and ZIF-8 possess very low selectivities, on the order of 3–4. The low CO_2/N_2 selectivity in MOF-5 and ZIF-8 further reduces their swing sorption performance from the idealized value listed in Table 2, making them much less applicable to flue gas CO_2 capture applications. Though detailed modelling would be required to better understand the cause for the enhanced swing capacities and selectivities in the open metal center MOFs, recent work has suggested that the improved performance derives from increased electrostatic interactions arising from the appreciable charge overlap between the framework and one of the CO_2 oxygens as compared to the weaker framework–CH_4 or N_2 interactions.[41,57]

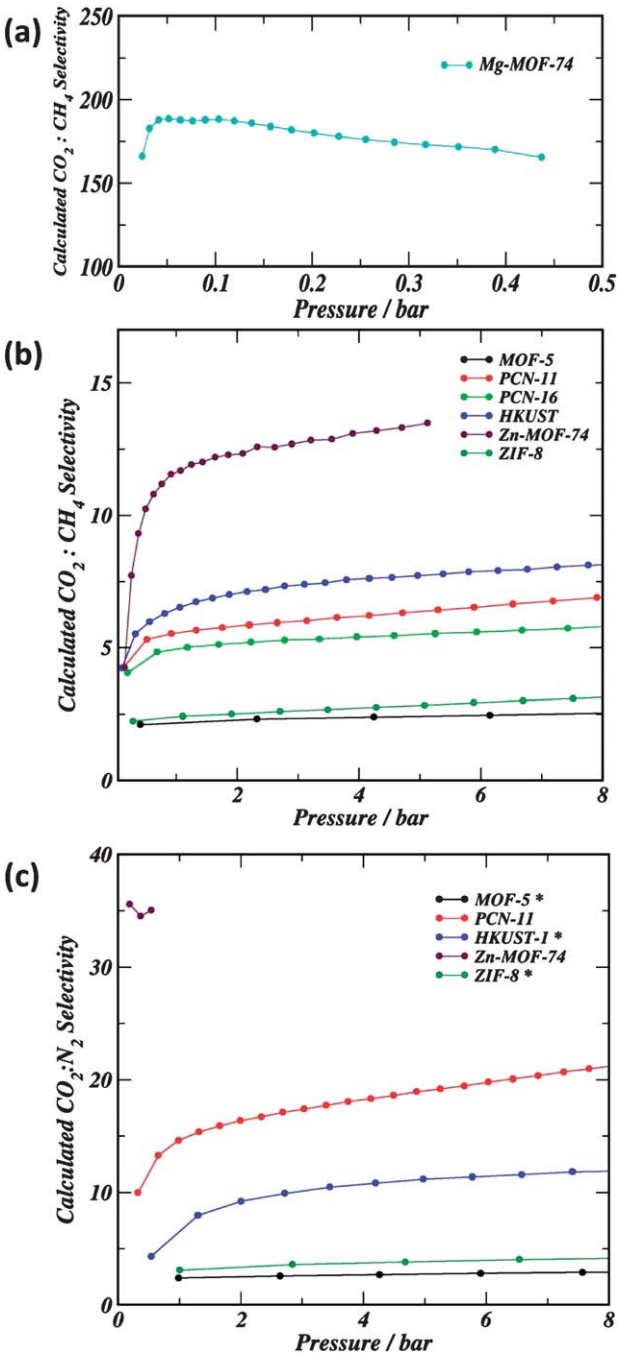

Fig. 5 Calculated selectivity in a range of MOFs near room temperature. (a) Calculated CO_2 to CH_4 selectivity in Mg–MOF-74, and (b) for the other MOFs investigated, assuming a 1 : 1 gas phase ratio. Note the large scale difference between Mg–MOF-74 and other MOFs. (c) Calculated CO_2 to N_2 selectivity at 300 K and 310 K (*) for select MOFs assuming a 1 : 4 CO_2 : N_2 gas phase ratio. In general, MOFs with open metal sites show higher selectivity than the high surface area materials, and improved selectivity at lower temperatures or higher pressures.

Conclusions

The primary purpose of this work is to highlight that optimizations of MOFs toward carbon capture and sequestration must take into account the process under which the capture will be achieved. We have shown that under typical swing adsorption processes that are widely used in industrial processing, an isosteric heat of adsorption between 22 kJ mol^{-1} and 28 kJ mol^{-1} is optimal for single-component CO_2 streams and between 26 kJ mol^{-1} and 31 kJ mol^{-1} for a 20% partial pressure CO_2 flue gas. We have also shown that several MOFs that contain open metal centers provide the proper isosteric heats, but that open metal centers can provide too strong of binding for certain applications. In addition to the proper isosteric heat, MOFs must possess sufficient surface area to yield significant capture capacities. Under high partial pressure CO_2 PSA conditions near room temperature, PCN-11 is shown to have the highest capture capacity of the MOFs studied here at 9 mmol g^{-1}, while Zn–MOF-74 shows the lowest capacity at 3.5 mmol g^{-1}. For VSA capture processes, HKUST-1 shows the highest capacity, with 6.4 mmol g^{-1}, as compared to ZIF-8 and MOF-5 at only 1 mmol g^{-1}. For typical flue gas conditions, where the partial pressure of CO_2 is typically between 10% and 20%, HKUST-1 becomes the most promising under PSA conditions, with a 4.5 mmol g^{-1} capacity, and the MOF-74 series dominates under VSA conditions. In order to place these performances in the context of the broader MOF field, we have also compared these MOFs to reports in the literature. Finally, we have looked at the CO_2/CH_4 and CO_2/N_2 sorption selectivity as a means of testing the CO_2 capture selectivity under a simulated mixed gas stream. Further experiments are underway to determine CO_2 selectivity compared to other flue gas impurities, in particular water, both by using IAST and single-component sorption isotherms as well as using mixed gas measurements.

Acknowledgements

We thank X.-S. Wang, S. Ma and H.-C. Zhou from Miami University of Ohio (now Texas A&M) for access to the PCN-11 and PCN-16 samples. This work was partially supported by the U. S. Department of Energy through BES grant no. DE-FG02-08ER46522 (T.Y.). J.M.S. acknowledges support from the National Research Council Postdoctoral Associate Program.

References

1 J. D. Figueroa, T. Fout, S. Plasynski, H. McIlvried and R. D. Srivastava, *Int. J. Greenhouse Gas Control*, 2008, **2**, 9.
2 R. S. Haszeldine, *Science*, 2009, **325**, 1647.
3 S. Ma and H.-C. Zhou, *Chem. Commun.*, 2010, **46**, 44.
4 K. M. Thomas, *Dalton Trans.*, 2009, 1487.
5 A. R. Millward and O. M. Yaghi, *J. Am. Chem. Soc.*, 2005, **127**, 17998.
6 P. L. Llewellyn, S. Bourrelly, C. Serre, A. Vimont, M. Daturi, L. Hamon, G. DeWeireld, J.-S. Chang, D.-Y. Hong, Y. K. Hwang, S. H. Jhung and G. Ferey, *Langmuir*, 2008, **24**, 7245.
7 B. Arstad, H. Fjellvag, K. O. Kongshaug, O. Swang and R. Blom, *Adsorption*, 2008, **14**, 755.
8 A. Demessence, D. M. D'Alessandro, M. L. Foo and J. R. Long, *J. Am. Chem. Soc.*, 2009, **131**, 8784.
9 S. R. Caskey, A. G. Wong-Foy and A. J. Matzger, *J. Am. Chem. Soc.*, 2008, **130**, 10870.
10 R. Vaidhyanathan, S. S. Iremonger, K. W. Dawson and G. K. H. Shimizu, *Chem. Commun.*, 2009, 5230.
11 M. T. Ho, G. W. Allinson and D. E. Wiley, *Ind. Eng. Chem. Res.*, 2008, **47**, 4883.
12 T. C. Merkel, H. Lin, X. Wei and R. Baker, *J. Membr. Sci.*, 2010, **359**, 126.
13 R. Banerjee, H. Furukawa, D. Britt, C. Knobler, M. O'Keeffe and O. M. Yaghi, *J. Am. Chem. Soc.*, 2009, **131**, 3875.
14 A. O. Yazaydin, R. Q. Snurr, T.-H. Park, K. Koh, J. Liu, M. D. LeVan, A. I. Benin, P. Jakubczak, M. Lanuza, D. B. Galloway, J. J. Low and R. R. Willis, *J. Am. Chem. Soc.*, 2009, **131**, 18198.
15 S. Cavenati, C. A. Grande, A. E. Rodrigues, C. Kiener and U. Muller, *Ind. Eng. Chem. Res.*, 2008, **47**, 6333.
16 S. Choi, J. H. Drese and C. W. Jones, *ChemSusChem*, 2009, **2**, 796.
17 M. Dinca and J. R. Long, *Angew. Chem., Int. Ed.*, 2008, **47**, 6766.
18 W. Zhou, *Chem. Rec.*, 2010, **10**, 200.
19 H. Li, M. Eddaoudi, M. O'Keeffe and O. M. Yaghi, *Nature*, 1999, **402**, 276.
20 K. S. Park, Z. Ni, A. P. Cote, J. Y. Choi, R. Huang, F. J. Uribe-Romo, H. K. Chae, M. O'Keeffe and O. M. Yaghi, *Proc. Natl. Acad. Sci. U. S. A.*, 2006, **103**, 10186.
21 X.-S. Wang, S. Ma, K. Rauch, J. M. Simmons, D. Yuan, X. Wang, T. Yildirim, W. C. Cole, J. J. Lopez, A. de Meijere and H.-C. Zhou, *Chem. Mater.*, 2008, **20**, 3145.
22 D. Sun, S. Ma, J. M. Simmons, J.-R. Li, D. Yuan and H.-C. Zhou, *Chem. Commun.*, 2010, **46**, 1329.
23 S. S. Y. Chui, S. M. F. Lo, J. P. H. Charmant, A. G. Orpen and I. D. Williams, *Science*, 1999, **283**, 1148.
24 B. Xiao, P. S. Wheatley, X. Zhao, A. J. Fletcher, S. Fox, A. G. Rossi, I. L. Megson, S. Bordiga, L. Regli and K. M. Thomas, *J. Am. Chem. Soc.*, 2007, **129**, 1203.
25 P. D. C. Dietzel, Y. Morita, R. Blom and H. Fjellvåg, *Angew. Chem., Int. Ed.*, 2005, **44**, 6354.
26 J. L. C. Rowsell and O. M. Yaghi, *J. Am. Chem. Soc.*, 2006, **128**, 1304.
27 P. D. C. Dietzel, V. Besikiotis and R. Blom, *J. Mater. Chem.*, 2009, **19**, 7362.
28 H. Wu, W. Zhou and T. Yildirim, *J. Am. Chem. Soc.*, 2009, **131**, 4995.
29 H. Wu, W. Zhou and T. Yildirim, *J. Phys. Chem. C*, 2009, **113**, 3029.
30 T. Yildirim and M. R. Hartman, *Phys. Rev. Lett.*, 2005, **95**, 215504.
31 W. Zhou, H. Wu, M. R. Hartman and T. Yildirim, *J. Phys. Chem. C*, 2007, **111**, 16131.
32 A. L. Myers and J. M. Prausnitz, *AIChE J.*, 1965, **11**, 121.
33 B. Liu and B. Smit, *Langmuir*, 2009, **25**, 5918.
34 Q. Yang and C. Zhong, *J. Phys. Chem. B*, 2006, **110**, 17776.
35 R. Babarao, Z. Hu, J. Jiang, S. Chempath and S. I. Sandler, *Langmuir*, 2007, **23**, 659.
36 Y. Liu, D. Liu, Q. Yang, C. Zhong and J. Mi, *Ind. Eng. Chem. Res.*, 2010, **49**, 2902.
37 K. S. Walton, A. R. Millward, D. Dubbeldam, H. Frost, J. J. Low, O. M. Yaghi and R. Q. Snurr, *J. Am. Chem. Soc.*, 2008, **130**, 406.
38 R. Krishna and J. M. van Baten, *Langmuir*, 2010, **26**, 3981.
39 Y. Liu, H. Kabbour, C. M. Brown, D. A. Neumann and C. C. Ahn, *Langmuir*, 2008, **24**, 4772.
40 P. D. C. Dietzel, R. E. Johnsen, H. Fjellvag, S. Bordiga, E. Groppo, S. Chavan and R. Blom, *Chem. Commun.*, 2008, 5125.
41 H. Wu, J. M. Simmons, G. Srinivas, W. Zhou and T. Yildirim, *J. Phys. Chem. Lett.*, 2010, **1**, 1946.
42 V. R. Choudhary and S. Mayadevi, *Langmuir*, 1996, **12**, 980.
43 Z. Liang, M. Marshall and A. L. Chaffee, *Energy Fuels*, 2009, **23**, 2785.
44 S. R. Miller, G. M. Pearce, P. A. Wright, F. Bonino, S. Chavan, S. Bordiga, I. Margiolaki, N. Guillou, G. Ferey, S. Bourrelly and P. L. Llewellyn, *J. Am. Chem. Soc.*, 2008, **130**, 15967.
45 L. Bastin, P. S. Barcia, E. J. Hurtado, J. A. C. Silva, A. E. Rodrigues and B. Chen, *J. Phys. Chem. C*, 2008, **112**, 1575.
46 S. Cavenati, C. A. Grande and A. E. Rodrigues, *J. Chem. Eng. Data*, 2004, **49**, 1095.
47 D. Shen, M. Bulow, F. Siperstein, M. Engelhard and A. L. Myers, *Adsorption*, 2000, **6**, 275.
48 B. Wang, A. P. Cote, H. Furukawa, M. O'Keeffe and O. M. Yaghi, *Nature*, 2008, **453**, 207.
49 S. K. Wirawan and D. Creaser, *Microporous Mesoporous Mater.*, 2006, **91**, 196.

50 S. K. Bhatia and A. L. Myers, *Langmuir*, 2006, **22**, 1688.
51 Y.-S. Bae and R. Q. Snurr, *Microporous Mesoporous Mater.*, 2010, **132**, 300.
52 A. L. Myers, *Colloids Surf., A*, 2004, **241**, 9.
53 Q. M. Wang, D. Shen, M. Bülow, M. L. Lau, S. Deng, F. R. Fitch, N. O. Lemcoff and J. Semanscin, *Microporous Mesoporous Mater.*, 2002, **55**, 217.
54 D. Britt, H. Furukawa, B. Wang, T. G. Glover and O. M. Yaghi, *Proc. Natl. Acad. Sci. U. S. A.*, 2009, **106**, 20637.
55 Z. Bao, L. Yu, Q. Ren, X. Lu and S. Deng, *J. Colloid Interface Sci.*, 2011, **353**, 549.
56 L. Hamon, E. Jolimaitre and G. D. Pirngruber, *Ind. Eng. Chem. Res.*, 2010, **49**, 7497.
57 W. Zhou and T. Yildirim, *J. Phys. Chem. C*, 2008, **112**, 8132.